

Article

Synthesis, Characterization and Catalytic Activity of UiO-66-NH₂ in the Esterification of Levulinic Acid

Daiana A. Bravo Fuchineco ¹, Angélica C. Heredia ¹, Sandra M. Mendoza ², Enrique Rodríguez-Castellón ^{3,*}
and Mónica E. Crivello ¹

- ¹ Centro de Investigación y Tecnología Química (CITeQ), Consejo Nacional de Investigaciones Científicas y Técnicas (CONICET), Facultad Regional Córdoba, Universidad Tecnológica Nacional (UTN-FRC), Córdoba 5016, Argentina; dbravo@frc.utn.edu.ar (D.A.B.F.); angelicaheredia@gmail.com (A.C.H.); mcrivello@frc.utn.edu.ar (M.E.C.)
- ² CONICET, Facultad Regional Reconquista, Universidad Tecnológica Nacional, Reconquista, Santa Fe 3560, Argentina; smendoza@frrq.utn.edu.ar
- ³ Departamento de Química Inorgánica, Cristalografía y Mineralogía, Universidad de Málaga (UMA), 29071 Málaga, Spain
- * Correspondence: castellon@uma.es

Abstract: The massive use of petroleum and its possible exhaustion are driving the current research trend to study alternative raw materials from biomass for organic reactions. In this context, the present article presents a study of the catalytic esterification of levulinic acid, a platform molecule, with ethanol. Metal-organic framework (MOF) type compounds UiO-66-NH₂ have been synthesized. Zirconium was incorporated, using zirconium chloride as a metal precursor, together with 2-aminoterephthalic acid as an organic binding agent. An alternative route of synthesis was proposed using more favorable conditions from an economic and environmental point of view, replacing dimethylformamide by 50 and 75% acetone as substitute solvent. The physicochemical properties of the materials were evaluated by X-ray diffraction (XRD), Infrared Spectrometry with Fourier Transform (FTIR), scanning electron microscopy (SEM), X-ray photoelectron spectroscopy (XPS), microwave plasma atomic emission spectroscopy (MP-AES) and N₂ adsorption to understand their morphology, crystalline, chemical and pore structure. The progress of the reaction was followed by gas chromatography and mass spectroscopy. The catalytic activity result of MOF_{25%} in autoclave reactor, showed 100% of selectivity to ethyl levulinate and a turnover number (TON) of 66.18 moles of product/moles of Zr. This good catalytic performance obtained by partial solvent replacement in the synthetic material provides a more economical and eco-friendly process for ethyl levulinate generation.

Keywords: metal-organic framework (MOF); UiO-66-NH₂; solvothermal; levulinic acid; esterification



Citation: Bravo Fuchineco, D.A.; Heredia, A.C.; Mendoza, S.M.; Rodríguez-Castellón, E.; Crivello, M.E. Synthesis, Characterization and Catalytic Activity of UiO-66-NH₂ in the Esterification of Levulinic Acid. *Appl. Nano* **2021**, *2*, 344–358. <https://doi.org/10.3390/applnano2040025>

Academic Editor: Michalis Konsolakis

Received: 17 November 2021
Accepted: 30 November 2021
Published: 10 December 2021

Publisher's Note: MDPI stays neutral with regard to jurisdictional claims in published maps and institutional affiliations.



Copyright: © 2021 by the authors. Licensee MDPI, Basel, Switzerland. This article is an open access article distributed under the terms and conditions of the Creative Commons Attribution (CC BY) license (<https://creativecommons.org/licenses/by/4.0/>).

1. Introduction

The increasing demand for chemicals and energy, together with the decline in oil resources, has led to great efforts to develop renewable replacements for fossil raw materials. The intensive use of fossil-fuel means that future energy demand, associated with increasing world populations, economic development and modernization cannot to be met [1–3].

The high production rate of lignocellulosic biomass and its low cost of raw material promise to be a source for the development of value-added products along with the energy generation [4].

It is well known that lignocellulosic biomass is mainly composed of cellulose (40–50 wt%), hemicellulose (25–30 wt%), and lignin (15–30 wt%) [5–8]. They are highly resistant to chemical and biological attacks due to the lignin coating around cellulose and hemicellulose. A crucial step in many transformation processes is the pretreatment stage so that the lignin coating is broken, allowing for the cellulose and hemicellulose hydrolysis, and the production of sugars.

The transformation of lignocellulosic biomass into platform molecules has become a key objective in the development of products with higher added value, which constitutes a crucial step towards the sustainable development of resources [3]. Levulinic acid derived from biomass is considered a platform building block due to its highly versatile structure for subsequent transformation into different valuable chemicals [9]. In particular, levulinate esters have low toxicity, high lubricity, flash point stability and moderate flow properties under low temperature conditions, which make them suitable additives for fuels [10]. Ethyl levulinate is usually synthesized using homogeneous acid catalysts such as H_2SO_4 , HCl and H_3PO_4 [11–14] causing inconveniences in catalyst recycling, products separation and environmental problems. Several heterogeneous acid catalysts such as zeolites (HUSY, HBEA, HMOR, HZSM-5, HMCM-22) [15], sulfated oxides like ZrO_2 [16] and SnO_2 [17], metallic salts [18], mesoporous silicates ($\text{SO}_3\text{H-SBA-15}$, Sn-TUD-1 , ZrAl-TUD-1 , $\text{WO}_3\text{-SBA-16}$, Al-MCM41) [19–26] have been studied for esterification reactions. The solid acid catalysts are an interesting alternative to overcome the drawbacks of homogeneous ones, as they can be easily separated from reaction mixtures and reused for repeated tests [27].

Metal-organic frameworks are porous crystalline organic-inorganic hybrid materials that consist of a regular array of positively charged metal ions surrounded by organic 'linker' molecules. The metal ions form nodes that bind the arms of the linkers together to form a repeating cage-like structure. Due to this hollow structure, MOFs have an exceptional large internal surface area [28,29]. The hybrid composition of inorganic/organic nature gives them characteristics and properties of both inorganic materials such as zeolites, and organic polymeric materials, presenting an ordered crystalline structure together with high porosity. An exceptional challenge in MOF synthesis is how to modify the chemical composition, functionality, and molecular dimensions systematically without altering the original topology [30,31].

The material UiO-66-NH_2 is formed by $\text{Zr}_6\text{O}_4(\text{OH})_4$ metal clusters composed of six zirconium atoms linked with the $\mu_3\text{-O}$ and $\mu_3\text{-OH}$ groups of the organic ligand 2-amino-terephthalate [32]. This MOF has a three-dimensional porous structure consisting of 9 Å octahedral porous cavities, connected to each other through windows of 6 Å diameter. The high degree of coordination of the metal cluster gives MOF a high chemical stability [33,34]. In this context, Abid et al. have reported the synthesis of amino-functionalized Zr-MOF nanoparticles by using different proportions of precursors and activation processes at various temperatures for their application in CO_2 and CH_4 adsorption [33]. Katz et al. have also reported a scalable and reproducible method of synthesizing UiO-66- and UiO-67- type MOFs, entailing the addition of HCl to the reaction mixture. This results in exceptional porosities, and works with a variety of linkers [35]. For their part, Cirujano et al. reported that UiO-66 and UiO-66-NH_2 are active and stable catalysts for the acid-catalyzed esterification of levulinic acid with EtOH , $n\text{-BuOH}$ and long-chain biomass-derived alcohols [36].

The modifications or improvements that are proposed in this work, with respect to what has already been published by other authors [37–42], consist in the synthesis of a MOF-type material UiO-66-NH_2 with a lower content of traditional N,N -dimethylformamide (DMF), which maintains its properties of crystallinity and porosity and that it can be used satisfactorily in esterification reactions of levulinic acid. Through the use of pressure reactors, both the conversion and selectivity to the desired product were improved, reducing the reaction time from 5 h (in batch) to 3 h (under pressure).

The aim of this work is to evaluate the activity of organic-metal frameworks (MOFs) in fine chemistry reactions, such as the esterification of levulinic acid with ethanol. For this purpose, the MOF Zr-UiO-66-NH_2 was synthesized by the solvothermal method, replacing part of the conventional solvent DMF with acetone as a less polluting solvent. Improvements were thus made to the synthesis method to obtain a material with high catalytic performance under more eco-friendly conditions.

2. Materials and Methods

2.1. Chemicals and Reagents

Analytical grade reagents were used for the preparation of catalysts and catalytic reactions. Zirconium chloride ($\geq 98\%$, Merck, Darmstadt, Alemania), aminoterephthalic acid ($\text{NH}_2\text{-BDC}$, 98% , Aldrich, Saint Louis, MO, USA), *N,N*-dimethylformamide (DMF, $\geq 99.8\%$, Biopack, Bs. As., Argentina) acetone (99.5% , Sintorgan, Bs. As., Argentina), ethanol ($\geq 99.5\%$, Biopack, Bs. As., Argentina) and levulinic acid (98% , Aldrich, Saint Louis, MO, USA) were used as received.

2.2. Synthesis of MOF UiO-66- NH_2

MOFs were obtained by a solvothermal method [36,40]. The DMF was replaced by 50 and 75% *v/v* acetone. The resulting samples were named as $\text{MOF}_{X\%}$ where "X" is the DMF content. The synthesis consisted of dissolving 1.027 g of ZrCl_4 in 50 mL of the solvent (DMF or DMF/acetone). The solution was magnetically stirred for 5 min. Then 0.789 g of aminoterephthalic acid ($\text{NH}_2\text{-BDC}$) were incorporated. The mixture was kept under magnetic stirring for 30 min. The gel was then transferred into a Teflon-lined stainless-steel autoclave and kept in an oven at $120\text{ }^\circ\text{C}$ for 24 h. The obtained material was immersed for 1 h in DMF and then washed with acetone, to exchange the DMF for a solvent with a lower boiling point, which can be easily removed. The solid was separated by filtration, affording a yellow powdery solid. Finally, the material was dried at $90\text{ }^\circ\text{C}$ for 24 h. In the cited bibliography, studies have been carried out with other metal precursors, in this case, the use of ZrCl_4 , as a source of Zr, is due to the fact that it is an active metal that allows obtaining good catalytic results in the esterification of levulinic acid. This is due to the type of Zr^{4+} coordination vacancy that is created when a linker molecule is missing, generating a good Lewis acid site needed to start the reaction [36,41,42].

2.3. Characterization of MOF UiO-66- NH_2

The XRD powder patterns were collected on an X'pert diffractometer (PANanalytical, Malvern, United Kingdom) using monochromatized Cu $\text{K}\alpha$ radiation ($\lambda = 1.54\text{ \AA}$) at a scan speed of $0.25^\circ\text{ min}^{-1}$ in 2θ .

Infrared analyses were carried out on a Smartomi-Transmission Nicolet iS10 spectrophotometer (Thermo Scientific, Waltham, MA, USA) in a range of $4000\text{--}400\text{ cm}^{-1}$.

Micrographs of the mixed oxides were obtained by scanning electron microscopy (SEM) using a model JSM-6380 LV instrument (JEOL, Lireweg, The Netherlands) equipped with a Supra 40 device (Carl Zeiss, Oberkochen, Germany). Samples were metallized with chromium.

The specific surface area (SSA), analysis was carried out in an ASAP 2020 instrument (Micromeritics, Norcross, GA, USA) and was calculated by the Brunauer–Emmett–Teller (BET) method. Prior to the determination of the adsorption isotherms, the samples were treated at $200\text{ }^\circ\text{C}$ during 60 min under 1.0×10^{-3} mbar vacuum. Regarding the analysis of adsorption-desorption isotherms, it was carried out by treating the sample with degassing at $200\text{ }^\circ\text{C}$ under vacuum. At temperatures above this, a collapse of the structure would occur due to the removal by calcination of the organic binder (aminoterephthalic acid) as analyzed by Hussein et al. [33].

X-ray photoelectron spectra (XPS) were recorded with a PHI VersaProbe II Scanning XPS Microprobe (Physical Electronics, Chanhassen, MN, USA) with scanning monochromatic X-ray Al $\text{K}\alpha$ radiation as the excitation source ($100\text{ }\mu\text{m}$ area analysed, 52.8 W , 15 kV , 1486.6 eV), and a charge neutralizer. The pressure in analysis chamber was maintained below 2.0×10^{-6} Pa. High-resolution spectra were recorded at a given take-off angle of 45° by a multi-channel hemispherical electron analyser operating in the constant pass energy mode at 29.35 eV . Spectra were charge referenced with the C 1s of adventitious carbon at 284.8 eV . Energy scale was calibrated using Cu $2p_{3/2}$, Ag $3d_{5/2}$, and Au $4f_{7/2}$ photoelectron lines at 932.7 , 368.2 , and 83.95 eV , respectively. The Multipack software version 9.6.0.15 was employed to analyze in detail the recorded spectra. The obtained spectra were fitted

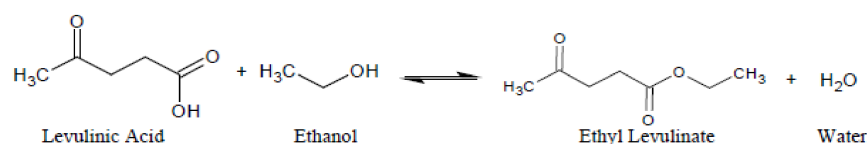
using Gaussian–Lorentzian curves to more accurately extract the binding energies of the different element core levels.

The elemental analysis was carried out by microwave plasma-atomic emission spectroscopy (MP-AES) on an Agilent 4200 instrument (Agilent, Santa Clara, CA, USA). Prior to elemental analysis, the samples were dissolved in nitric acid (65%) for 10 min in a microwave oven (SCP Science, Baie-D'Urfe, QC, Canada).

To assess surface acidity, the CO adsorbed during 2 h at room temperature was measured by FTIR analysis at 50 and 100 °C on the Nicolet iS10 instrument. The material was previously treated under vacuum.

2.4. Catalytic Esterification Reaction

The performance of the Zr-MOF catalysts was then evaluated in the esterification reaction (Scheme 1). Ten mL of ethanol (E) mixed with levulinic acid (LA, molar ratio 1:15) were put in contact with 0.05 g of the prepared catalyst. Two reaction systems, a batch reactor with reflux condenser and a Teflon-lined stainless-steel autoclave, were employed in this study and compared for LA conversion efficiency. The reaction mixture in reactor with reflux condenser was magnetically stirred at 78 °C [17,19,36,41–44]. On the other hand, autoclave was sealed and purged three times with high purity N₂, and pressurized to 30 bar, before to reaction mixture was heated at 180 °C inside a conventional oven with magnetic stirring at 400 rpm.



Scheme 1. Esterification Reaction.

The reaction was allowed to occur for 5 h and 0.15 mL of samples were collected from the reaction medium at 0, 1, 2, 3, 4 and 5 h. Time $t = 0$ h was the time at which the temperature of the reaction medium reached 78 °C or 180 °C. Samples were collected using a microsyringe equipped with a filter (Whatman paper filter n° 5) to remove catalyst particles. The reaction mixture was analyzed by gas chromatography on an Agilent Technologies 7820A instrument equipped with a HP-20M column and a FID detector, and by mass spectroscopy on a Clarus 560 instrument (Perkin Elmer, Hopkinton, MA, USA).

After the reaction was finished, the catalyst was separated from the reaction medium by centrifugation; then it was washed again with acetone and dried at 90 °C overnight, for further use.

The LA conversion, selectivity, yield and TON of products are calculated based on a mass balance at the reactor outlet as follows:

$$\% \text{ Conversion} = \frac{n_{I \text{ LA}} - n_{F \text{ LA}}}{n_{I \text{ LA}}} \times 100 \quad (1)$$

$$\% \text{ Selectivity} = \frac{n_{\text{main product}}}{n_{I \text{ LA}} - n_{F \text{ LA}}} \times 100 \quad (2)$$

$$\% \text{ Yield} = \frac{\text{Conversion} \times \text{Selectivity}}{100} \quad (3)$$

$$\text{TON} = \frac{\text{mole of EL}}{\text{mole of Zr}} \quad (4)$$

where $n_{I \text{ LA}}$ and $n_{F \text{ LA}}$ are the initial and final concentrations of levulinic acid, $n_{\text{main product}}$ is that corresponding to the concentration of ethyl levulinate.

3. Results

3.1. Physicochemical Characterization

3.1.1. X-ray Diffraction

Figure 1 shows the X-ray diffraction patterns of the MOFs with different DMF contents (25, 50 and 100%). Two peaks located near 2θ of 7.4 and 8.5° are associated to the diffraction by (111) and (200) planes characteristic of the MOF UiO-66-NH₂. It was observed that all the materials present a good order and crystallinity, except the MOF_{50%} sample that presents a lower peak intensity, which is related to the crystalline defects of the material that provide its acidity. This will be discussed in Section 3.1.6 acid analysis by FTIR-CO. The diffraction patterns show similar behaviors, independently of the substitution of the DMF solvent by acetone [45–50].

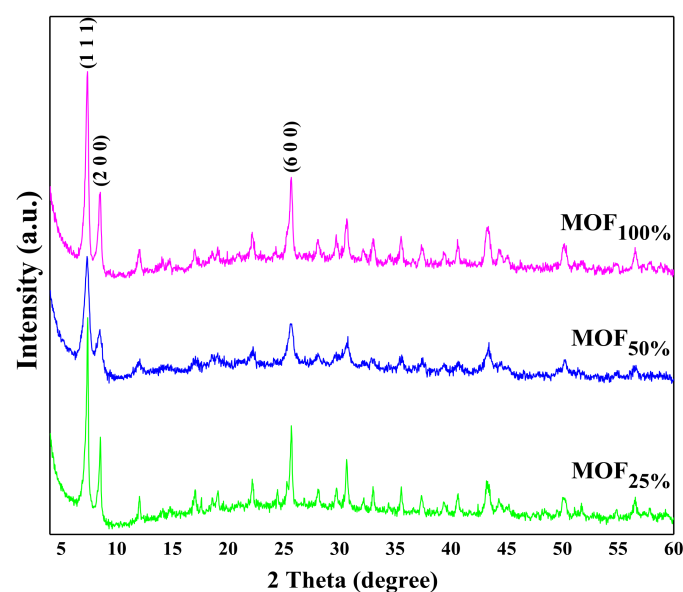


Figure 1. X-ray diffraction patterns for MOFs with different DMF contents.

3.1.2. FTIR Spectroscopy

The MOFs FTIR spectra are shown in Figure 2. The signals at 3447 and 3354 cm^{-1} corresponded to the symmetric and asymmetric stretching bands of the amine moiety, while the signals at 1257 and 1385 cm^{-1} are attributed to C-N binding absorptions. The COO⁻ group presents bands at 1571 and 1436 cm^{-1} , assigned to the corresponding symmetric and asymmetric stretching vibrations and the benzene ring C=C bonds showed a band at 1494 cm^{-1} . The two lowest frequencies at 573 and 475 cm^{-1} were assigned to Zr-O stretching in the MOF clusters [51–53]. Regarding the series of materials, it can be noted that the MOF_{50%} shows a higher intensity in the peaks corresponding to the N-H and Zr-O bond, both functional groups necessary to generate the dual acid-base mechanics for the esterification reaction. This is also related to the higher contribution of these elements seen through in the XPS analysis (Section 3.1.5).

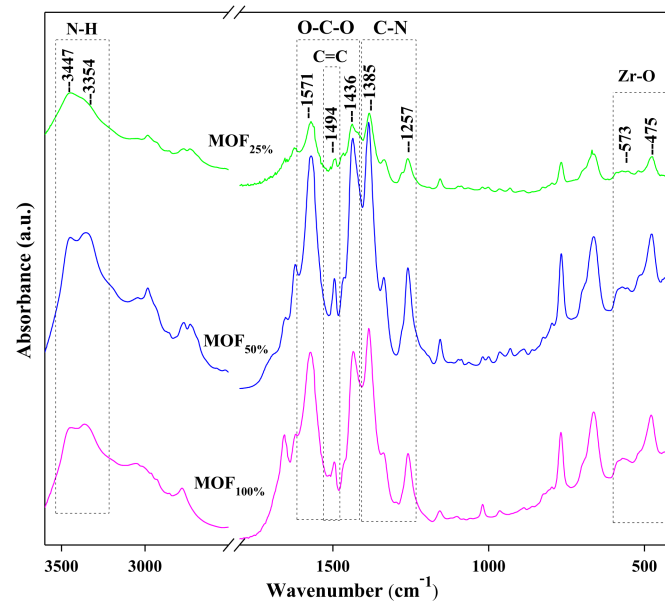


Figure 2. FTIR spectra for MOFs with different DMF contents.

3.1.3. SEM-EDS Analysis

The SEM images of UiO-66-NH₂ (Figure 3) show randomly aligned spherical particles, with an average particle size from ~153 nm (MOF_{100%}) to ~224 nm (MOF_{25%}, Figure S1). The MOF_{100%} crystals are smaller and more dispersed than those obtained by replacing DMF for acetone, in which the small crystals agglomerate constituting a well-defined spheric topology [54–56].

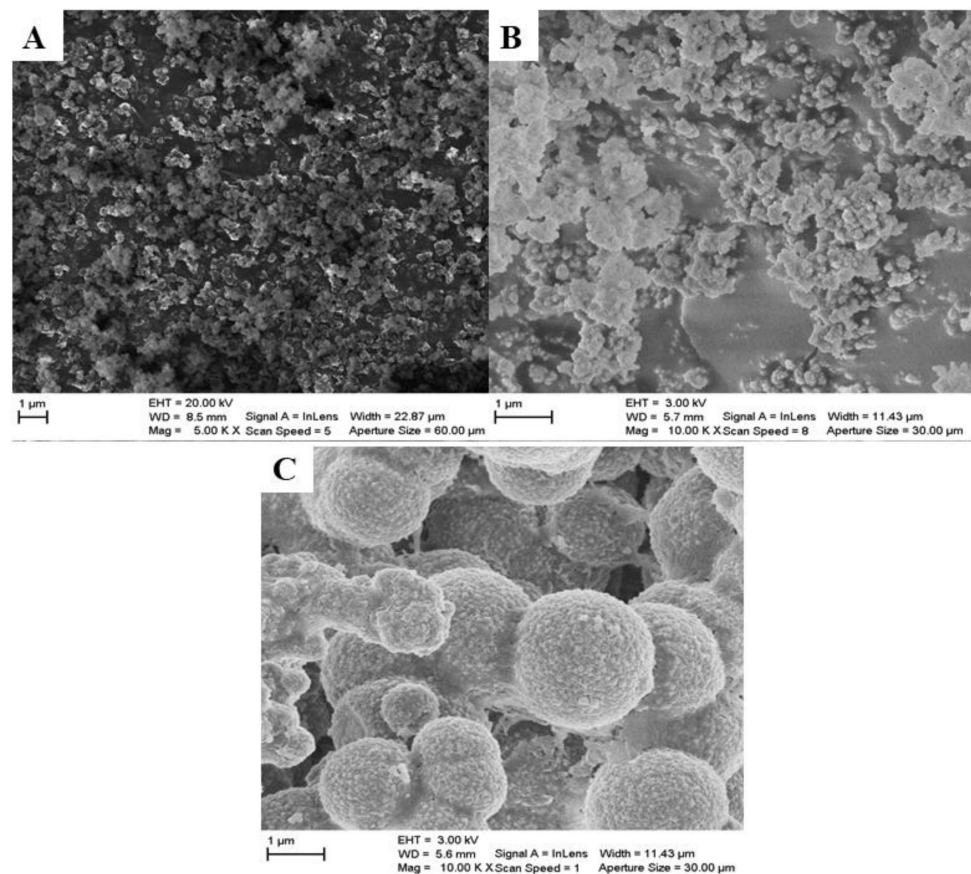


Figure 3. SEM image of the MOF_{100%} (A), MOF_{50%} (B) and MOF_{25%} (C).

The elemental mapping verified the presence and dispersion of Zr atoms that belong to the metal salt and C, O and N atoms contributed by the organic ligand. Figure 4 shows images corresponding to the homogeneous distribution of these elements on the surface in MOF_{100%}. In the rest of the samples, the dispersion of the elements on the surface was similar.

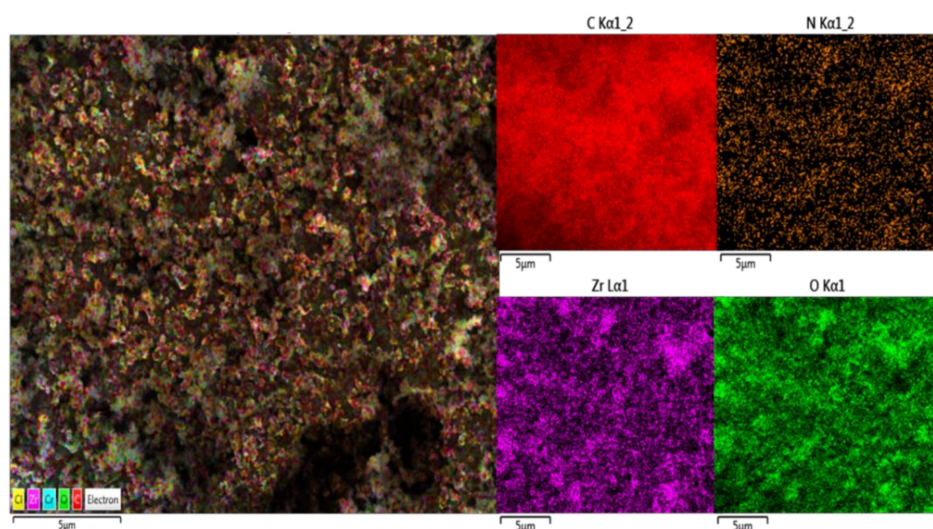


Figure 4. SEM elemental mapping of the MOF_{100%} sample.

3.1.4. Microwave Plasma Atomic Emission Spectrometry (MP-AES) and Surface Area by BET

Table 1 shows the content of Zr (wt%) in the synthesized samples. In most cases the Zr content was approximately 54–66 wt% of the theoretical value (31 wt%). While the MOF_{25%} sample presented half of the Zr theoretical content. The main difference between the values of wt% is due precisely to the replacement of DMF by acetone, because DMF is a more polar solvent, it facilitates the complete dissociation of the ZrCl₄ and the metal union with the organic binder, allowing it to more easily form the structure of the MOFs [33]. The commonly used DMF has an active role in UiO-66-NH₂ synthesis by entering the coordination sphere of the zirconium, steering the formation of the crystal lattice formation [57].

Table 1. Elemental analysis and surface area.

Catalyst	Zr (wt%) Nominal	Zr (wt%) Experimental	BET (m ² g ⁻¹)	Pore Size (nm)	Micropore Area (m ² /g)	Mesopore Area (m ² /g)
MOF _{100%}	31	20.5 ± 0.4	474 ± 12	3.60	168 ± 4	219 ± 5
MOF _{50%}	31	21.0 ± 0.4	424 ± 22	2.34	179 ± 4	156 ± 4
MOF _{25%}	31	16.8 ± 0.3	407 ± 24	1.15	216 ± 5	151 ± 4

The MOF_{100%} sample showed the highest value of surface area (Table 1). A tendency of the surface area and mesopore area to increase with the DMF content was observed. The increased BET area can be observed in the SEM images where the structures become more compact and closed with the increase of the acetone content. When analyzing the pore size, it is observed that it decreases as the DMF is replaced; as the solvent is the one that gives the internal structure of the pore, when changing it for acetone (smaller molecule) its size is reduced, this effect promotes the high number of small sized pores and their micropore area was increased.

From the adsorption data analysis, these materials have been found to be microporous and mesoporous. The physisorption isotherms behavior of the MOFs, according to the IUPAC classification, can be assigned to type Ib, with H1 for MOF_{100%} and MOF_{50%} while the

MOF_{25%} shows H4 hysteresis loops, that are often found in micro-mesoporous materials. The pore size presented a wide range values between ~1 and ~3.6 nm and was associated to wider microporosity and narrow mesoporosity in the materials (Figure 5) [58–61]. The MOF_{100%} and MOF_{50%} samples show an increase in the uptake in the pressure range ($p/p_0 > 0.9$) and the hysteresis between the adsorption and desorption branches is characteristic of mesopores. The sample MOF_{25%} which was synthesized with a lower DMF content, shows an increase in adsorption in the low-pressure range ($p/p_0 < 0.3$), suggesting the existence of micropores [62]. These behaviours suggest that increasing the DMF replacement by acetone has a significant influence on pore structures by promoting increased microporosity.

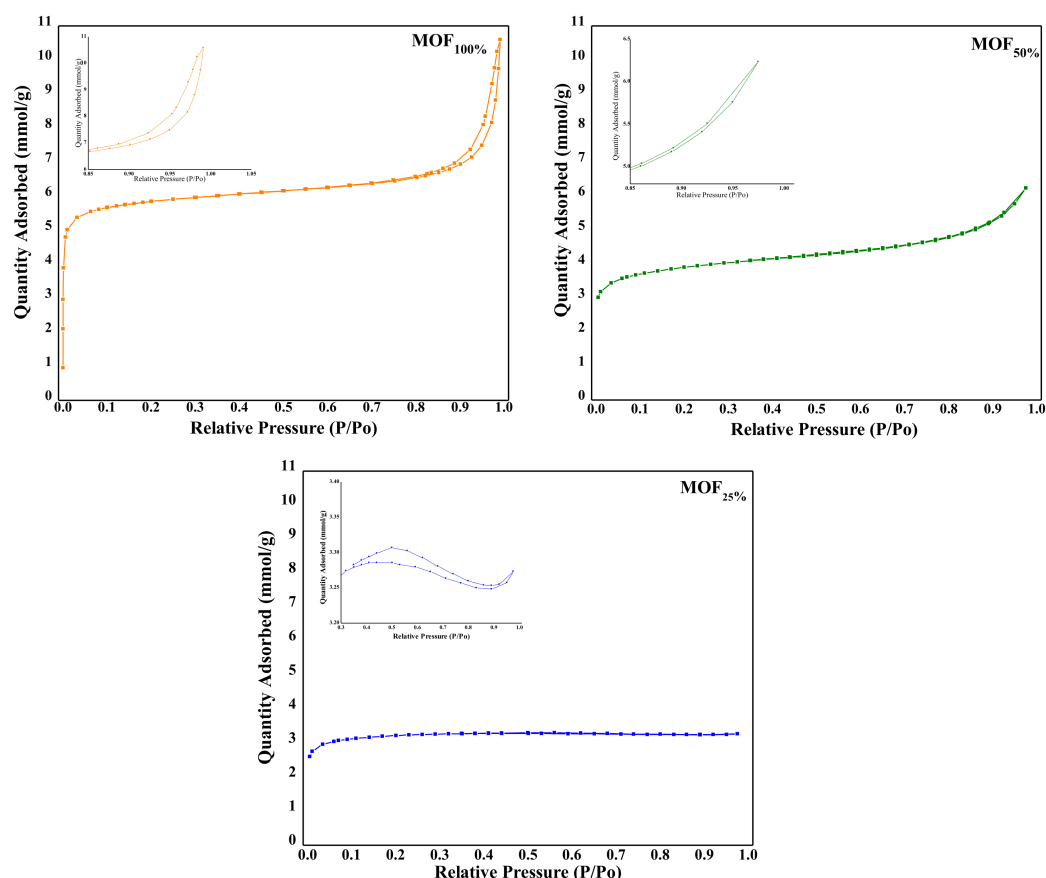


Figure 5. N₂ adsorption–desorption isotherms at $-196\text{ }^{\circ}\text{C}$.

3.1.5. XPS-Spectroscopy

The catalysts were studied by XPS to know their surface chemical composition and the chemical state of the different constituent elements. Table 2 lists the surface chemical composition and it can be observed that the MOF_{50%} sample exhibits the highest Zr content as also it was shown in the bulk above. Another relevant fact is that there is a direct relationship between the N content and the C content. With these data we can see that MOF_{25%} sample presents the highest N and C percentages indicating a high surface presence of grafted aminoterephthalic moieties, and the MOF_{50%} sample the lowest one. The higher surface Zr content of sample MOF_{50%} is a consequence of the lower surface presence of amino compound. All the samples contain some Cl impurities.

Table 2. Surface chemical composition (in atomic concentration %) of the studied catalysts determined by XPS.

Sample	C%	N%	O%	Zr%
MOF _{100%}	60.54	4.62	29.87	4.97
MOF _{50%}	51.95	3.85	36.33	7.87
MOF _{25%}	67.11	7.61	22.36	2.92

Table 3 presents the binding energy values of the constituent elements of the catalysts, and Figure 6 the C 1s, N 1s and O 1s core level spectra. The C 1s core level spectra (Figure 6) can be decomposed into three contributions at 284.8, 286.1 and 288.8 eV. The contribution at 284.8 eV is assigned to adventitious carbon, and -C-C- and -C=C- bonds. The second contribution at 286.1 eV is derived from C-N and C-OH bonds, and finally the contribution at high binding energy to the presence of carboxylate and carboxylic groups [63]. More interesting is the analysis of the N 1s core level spectra (Figure 6). These N 1s spectra can be deconvoluted into three contributions; the first at low binding energy (399.3 eV) is assigned to amide groups, while those at about 400.4 and 401.8 eV to the amino and protonated amino groups from the aminoterephthalic group [64]. The N 1s spectrum of sample MOF_{50%} shows, as expected, the lowest relative intensities of the contributions at 400.4 and 401.8 eV derived from the presence of aminoterephthalic. Also, as expected, the N 1s spectrum of sample MOF_{25%}, which presents the higher content of aminoterephthalic, presents the highest relative intensities of the contributions at 400.5 and 402.0 eV. The Zr 3d core level spectra of the three samples show the typical Zr 3d_{5/2}-Zr 3d_{3/2} doublet with Zr 3d_{5/2} binding energy values at 182.9 eV assigned to Zr⁴⁺ [65].

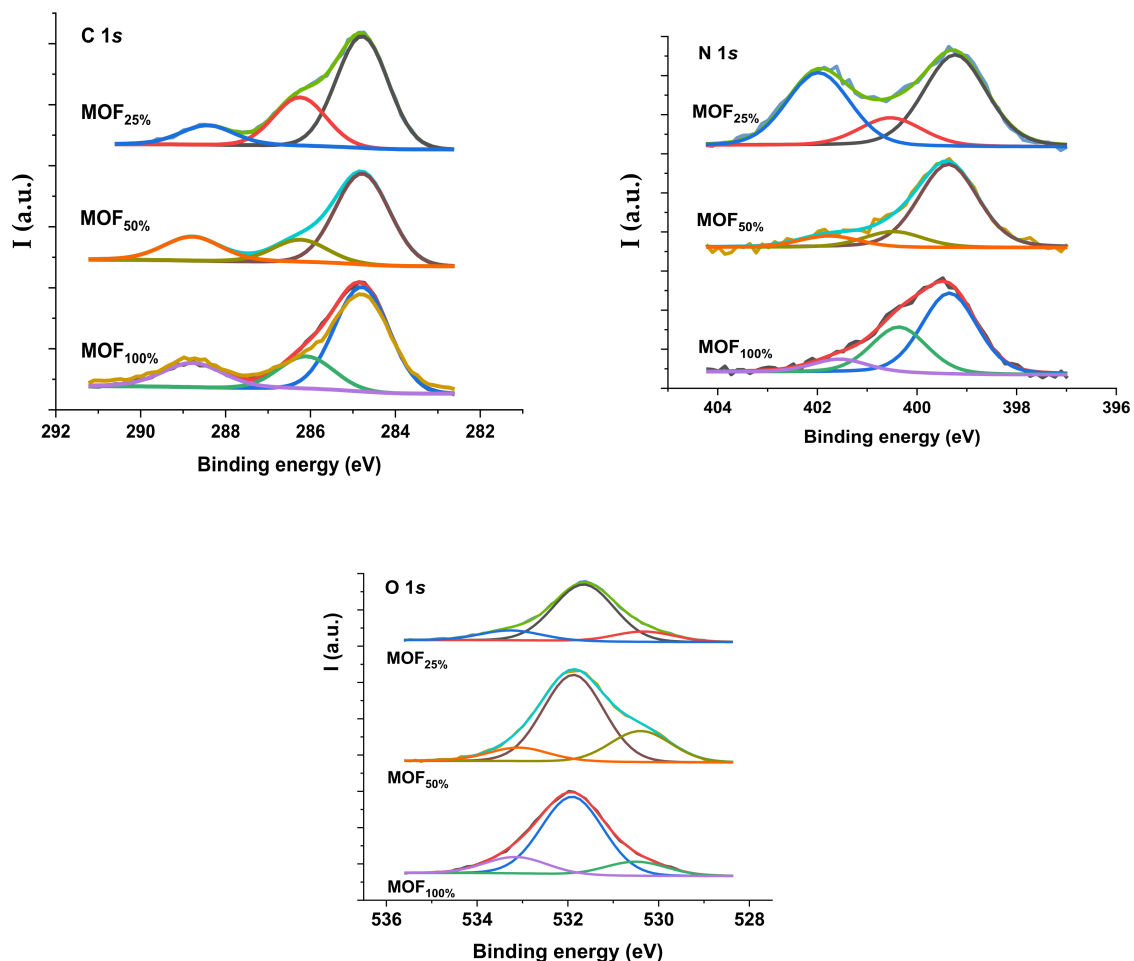
**Figure 6.** C 1s, N 1s and O 1s core level spectra for samples MOF_{100%}, MOF_{50%} and MOF_{25%}.

Table 3. Binding energy values (in eV) of different elements for the studied catalysts. Area percentages are indicated in parentheses.

Sample	C 1s	N 1s	O 1s	Zr 3d _{5/2}
MOF _{100%}	284.8 (62)	399.3 (57)	530.5 (13)	182.9
	282.1 (20)	400.4 (33)	531 (15)	
	288.8 (18)	401.6 (10)	533.2 (15)	
MOF _{50%}	284.8 (64)	399.4 (76)	530.4 (24)	182.9
	286.2 (16)	400.5 (14)	531.9 (65)	
	288.8 (20)	401.8 (10)	533.1 (11)	
MOF _{25%}	284.8 (61)	399.2 (48)	530.3 (13)	182.9
	286.2 (27)	400.5 (15)	531.6 (74)	
	288.4 (12)	402.0 (15)	533.3 (13)	

3.1.6. Acid Analysis by FTIR-CO

Table 4 shows the relative area percentage corresponding to the Lewis and Brønsted acid sites measured by FTIR CO adsorbed at different temperatures (50 and 100 °C). The graphs are attached in the Supplementary Materials (Figure S2). The acid sites measured at low temperature are defined as weak, while those measured at high temperature are defined as medium [37]. It is well-known that the Lewis acid sites in UiO-66-NH₂ come from vacancies associated with the thermal elimination of water molecules binding to metallic nodes ([Zr₆O₄(OH)₄]¹²⁺ clusters to [Zr₆O₆]¹²⁺) and the crystalline defect associated to the NH₂-BDC binding lack [42]. The Lewis acid sites can be related to pore volume, vacancies and crystalline defects in the structure, this generating a high internal area and enhances the Zr⁴⁺ availability. Furthermore, as these materials have an amino group (NH₂) that come from the organic binder, they present associated basic sites, necessary to generate the acid-base duality in the catalyst [36].

Table 4. FTIR of CO adsorbed.

Sample	% Area (50 °C) Weak Sites		% Area (100 °C) Medium Sites		% Area Total Sites	
	Lewis	Brønsted	Lewis	Brønsted	Lewis	Brønsted
MOF _{100%}	55.38	44.62	50.23	49.77	52.81	47.19
MOF _{50%}	69.32	30.68	50.29	49.71	59.81	40.20
MOF _{25%}	48.35	51.65	45.86	54.14	47.11	52.90

The higher Zr⁴⁺ availability and presence of amino group (NH₂) on the surface were also corroborated by XPS in the samples MOF_{50%} and MOF_{25%}, respectively (see Table 2).

3.2. Catalytic Activity: Esterification for Ethyl Levulinate Production

The esterification reaction was evaluated for the different MOF_x samples. The main esterification product was ethyl levulinate (EL) and the byproduct was the corresponding β-lactone obtained by the dehydration of levulinic acid. A blank batch reaction was performed without catalyst, the observed conversion value (1.45%) was then used to fit the catalytic activity data. The main product observed, in this case, was β-lactone. This may be because of the acidic character of LA, which can autocatalyze the reaction to a certain extent [36]. For the case of the autoclave reaction, the blank showed a conversion of 20%, with a higher selectivity towards the ester. Autoclave reactor catalytic results showed better performance than the batch system, with 100% of selectivity for all materials (Tables 5 and 6). The MOF_{50%} and MOF_{25%} samples presented the highest conversion and the best yield to EL in a batch reactor, and autoclave reactor, respectively. Pressure and temperature enhance the diffusion of molecules inside the pores and reaching of the internal active sites, improving the catalytic performance in the autoclave reactor [49].

Table 5. Catalytic activity in Batch. T = 78 °C, 0.05 g catalyst.

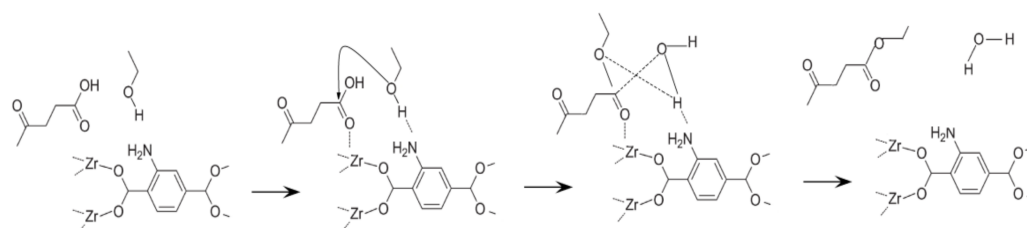
Catalyst	Conversion %	Selectivity EL %	TON
MOF _{100%}	12.85	40.75	3
MOF _{50%}	20.07	46.66	5.21
MOF _{25%}	18.37	24.65	3.14

Table 6. Catalytic activity in autoclave. T = 180 °C, p = 30 bar, 0.05 g catalyst.

Catalyst	Conversion %	Selectivity EL %	TON
MOF _{100%}	96.16	100	54.25
MOF _{50%}	96.09	100	53.01
MOF _{25%}	96.20	100	66.18
MOF _{25%} Reuse	97.66	88.96	59.77

In the bibliography related to reactions to obtain ethyl levulinate using pressure reactors, we can mention the results and contributions of Negus et al. [37], Peixoto et al. [38] and Tukacs et al. [39], where the conditions are 300 °C for 6 h. In this work milder conditions of temperature and pressure are used, obtaining good catalytic yields in shorter reaction times.

A dual acid-base activation mechanism was previously proposed [36], which the Zr sites interact with adsorbed LA while the amino group, close to the Zr, forms a hydrogen bonded adduct with the alcohol, increasing the nucleophilic character of the O atom and thus favoring the first reaction step. By XPS, MOF₂₅ showed a highest N content in -NH₂ groups which would indicate more basic sites, while MOF₅₀ contains a highest percentage of surface-available Zr⁴⁺, which means a higher percentage of acidic sites. The low performance obtained with MOF_{100%} compared with MOF_{50%} (7.87% Zr) and MOF_{25%} (7.61% N) in a batch system, may be related to the Zr and N at the surface as the XPS data showed. A cooperative action of the (basic) amino groups that are located adjacent to the (acid) Zr sites of UiO-66-H₂, leads to a bifunctional acid-base catalyst. Scheme 2 shows a possible esterification mechanism. Levulinic acid increases the electrophilic character of the carboxylic carbon atom, by coordinating with the Zr acid sites. On the other hand, the alcohol forms a hydrogen bond to the amino group, which increases the nucleophilic character of his O atom and promotes a nucleophilic attack on the carboxylic carbon.

**Scheme 2.** Mechanism of esterification of LA with ethanol on a MOF UiO-66-NH₂.

The reusability of MOF_{25%} catalyst was investigated for the esterification of LA. The catalyst was recycled as described by the following procedure. At the end of the LA esterification run, the catalyst was separated from the reaction mixture using high-speed centrifugation. The obtained catalyst was thoroughly washed with acetone to remove the adsorbed species. Then the recycled catalyst was dried for 12 h before used for the next run under identical reaction conditions. The results are shown in Table 6, where the conversion was increased to 97.66% while the selectivity decreased to 88.96%. The high TON value obtained with MOF_{25%}, shows that good catalytic results can be obtained with a synthesized catalyst under more environmentally friendly conditions.

The XRD patterns of used catalysts were recorded and compared with the fresh ones to demonstrate that their crystallinity is retained. This is shown in the Supplementary Materials (Figures S3 and S4).

3.3. Estimation of Kinetic Parameters

The esterification reaction of LA in the presence of E to produce EL and water was shown in Equation (1). A pseudo-homogeneous model was chosen to represent the reaction kinetics, considering an irreversible reaction [36,66–68]. The rate equation for this reaction could be thus expressed as follows (Equation (5)). The adjustment was made with the experimental data obtained in the reaction catalyzed by the MOF_{50%} material:

$$r_A = -\frac{dC_A}{dt} = k [LA] [E] \quad (5)$$

Furthermore, since ethanol is always in excess, the reaction was assumed to be zero order with respect to it (Ostwald isolation method) and the expression becomes Equation (6), where k (min^{-1}) is the rate constant for the forward reaction:

$$\frac{dC_A}{dt} = k[LA] \quad (6)$$

The integrated form of Equation (6) can be expressed as:

$$\text{Ln}[LA_t] = -kt + \text{Ln}[LA_0] \quad (7)$$

where $[LA_0]$ and $[LA_t]$ indicate the initial concentration of LA ($\text{mol}\cdot\text{L}^{-1}$) and at any time t , respectively. On the other hand, k is the slope and $\text{Ln}[LA_0]$ the intercept in a plot of $\text{Ln}[LA_t]$ versus t .

The experimental data of the OC reactions were fitted to the model represented by Equation (7), and the analysis performed with pseudo-first order kinetics in the esterification reaction of LA shows very good correlation values. This adjustment gives a kinetic constant value $k = 7.627 \times 10^{-4} \text{ min}^{-1}$ with an R^2 of 0.98. Additional data have been included in the Supplementary Materials (Table S1 and Figure S5).

4. Conclusions

The synthesis of the MOF UiO-66-NH₂ was achieved under mild solvothermal conditions, replacing up to 75% *v/v* of the traditional dimethylformamide with acetone. XRD and SEM analyses showed good crystallinity and morphology in the synthesized samples. The Zr content in the synthesized samples was ~65% of the theoretical value. A pore size between ~1 and ~3 nm was measured and associated to micro- and mesoporosity in the materials. The Zr⁴⁺ species coordinated in an O-Zr-O environment, the C in the organic matrix and the N in the amino and protonated amino group were observed by XPS analysis. Weak and medium Lewis and Brønsted acidity sites were identified by FTIR of adsorbed CO. The acid site is related to the crystalline structure defects, leading to increased availability of the Zr⁴⁺ inside the pore and on the surface. Regarding the kinetic model of the esterification reaction, it can be said that an adjustment was achieved with pseudo first order kinetics, with an R^2 of 0.98 and the value of the reaction constant k was $7.627 \times 10^{-4} \text{ min}^{-1}$. Autoclave reactor catalytic results showed better TON values than the batch system for all materials. Pressure and temperature promoted the diffusion of molecules inside the pores and access to internal active sites, improving the catalytic performance, a dual interaction between substrates and the Lewis acid contributed by the available Zr⁴⁺ together to the amino group, as well inside the pore as on the catalyst surface, promote the esterification reaction. Therefore, autoclave optimal reaction conditions plus a partial solvent replacement on material synthesis appear as a promising alternative for ethyl levulinate production under more economical and eco-friendly processes.

Supplementary Materials: The following are available online at <https://www.mdpi.com/article/10.3390/applnano2040025/s1>. Additional information about the particle size, the XRD pattern for the used catalyst, the CO-FTIR absorption spectra, the kinetics of the reaction and the adjustments made has been included in the file supplied as Supplementary Materials.

Author Contributions: Conceptualization, A.C.H. and M.E.C.; methodology, D.A.B.F.; validation, A.C.H., M.E.C. and D.A.B.F.; formal analysis, E.R.-C., S.M.M., A.C.H., M.E.C. and D.A.B.F.; investigation, E.R.-C., S.M.M., A.C.H., M.E.C. and D.A.B.F.; writing—original draft preparation, D.A.B.F.; writing—review and editing, A.C.H., M.E.C. and E.R.-C.; supervision, M.E.C. and E.R.-C. All authors have read and agreed to the published version of the manuscript.

Funding: Projects PID-UTN-SCyT (MATCBCO 008094TC) Universidad Tecnológica Nacional. Projects RTI2018-099668-BC22 of Ministerio de Ciencia, Innovación y Universidades, and UMA18-FEDERJA-126 and P20_00375 of Junta de Andalucía and FEDER funds.

Institutional Review Board Statement: Not applicable.

Informed Consent Statement: Not applicable.

Data Availability Statement: This statement is excluded.

Acknowledgments: Financial support from the Consejo Nacional de Investigaciones Científicas y Tecnológicas (CONICET) and Universidad Tecnológica Nacional—Facultad Regional Córdoba (UTN-FRC). ERC thanks to projects RTI2018-099668-BC22 of Ministerio de Ciencia, Innovación y Universidades, and UMA18-FEDERJA-126 and P20_00375 of Junta de Andalucía and FEDER funds.

Conflicts of Interest: The authors declare no conflict of interest.

References

1. Dhyani, V.; Bhaskar, T. A comprehensive review on the pyrolysis of lignocellulosic biomass. *Renew. Energy* **2018**, *129*, 695–716. [[CrossRef](#)]
2. Badgujar, K.C.; Bhanage, B.M. Factors governing dissolution process of lignocellulosic biomass in ionic liquid: Current status, overview and challenges. *Bioresour. Technol.* **2015**, *178*, 2–18. [[CrossRef](#)]
3. Mikola, M.; Ahola, J.; Tanskanen, J. Production of levulinic acid from glucose in sulfolane/water mixtures. *Chem. Eng. Res. Des.* **2019**, *148*, 291–297. [[CrossRef](#)]
4. De Bhowmick, G.; Sarmah, A.K.; Sen, R. Lignocellulosic biorefinery as a model for sustainable development of biofuels and value added products. *Bioresour. Technol.* **2018**, *247*, 1144–1154. [[CrossRef](#)]
5. Comba, M.B.; Tsai, Y.H.; Sarotti, A.M.; Mangione, M.I.; Suárez, A.G.; Spanevello, R.A. Levoglucosenone and its new applications: Valorization of cellulose residues. *Eur. J. Org. Chem.* **2018**, *5*, 590–604. [[CrossRef](#)]
6. Wang, H.; Guo, Y.; Chang, C.; Zhu, X.; Liu, X.; Han, J.; Ge, Q. Enhancing tungsten oxide/SBA-15 catalysts for hydrolysis of cellobiose through doping ZrO₂. *Appl. Catal. A Gen.* **2016**, *523*, 182–192. [[CrossRef](#)]
7. Sheldon, R.A. Green and sustainable manufacture of chemicals from biomass: State of the art. *Green Chem.* **2014**, *16*, 950–963. [[CrossRef](#)]
8. Shen, S.; Wang, C.; Han, Y.; Cai, B.; Li, H. Influence of reaction conditions on heterogeneous hydrolysis of cellulose over phenolic residue-derived solid acid. *Fuel* **2014**, *134*, 573–578. [[CrossRef](#)]
9. Lin, T.Y.; Lin, K.Y.A. Microwave-enhanced catalytic transfer hydrogenation of levulinic acid to γ -valerolactone using zirconium-based metal organic frameworks: A comparative study with conventional heating processes. *J. Taiwan Inst. Chem. Eng.* **2019**, *96*, 321–328. [[CrossRef](#)]
10. Ogino, I.; Suzuki, Y.; Mukai, S.R. Esterification of levulinic acid with ethanol catalyzed by sulfonated carbon catalysts: Promotional effects of additional functional groups. *Catal. Today* **2018**, *314*, 62–69. [[CrossRef](#)]
11. Xu, G.; Chang, C.; Zhu, W.; Li, B.; Ma, X.J.; Du, F.G. A comparative study on direct production of ethyl levulinate from glucose in ethanol media catalysed by different acid catalysts. *Chem. Pap.* **2013**, *67*, 1355–1363. [[CrossRef](#)]
12. Bart, H.J.; Reidetschlager, J.; Dchatka, K.; Lehmann, A. Kinetics of esterification of levulinic acid with n-butanol by homogeneous catalysts. *Ind. Eng. Chem. Res.* **1994**, *33*, 21–25. [[CrossRef](#)]
13. Omoruyi, U.; Page, S.; Hallett, J.; Miller, P.W. Homogeneous Catalyzed Reactions of Levulinic Acid: To γ -Valerolactone and Beyond. *ChemSusChem* **2016**, *9*, 2037–2047. [[CrossRef](#)] [[PubMed](#)]
14. Mehdi, H.; Fábos, V.; Tuba, R.; Bodor, A.; Mika, L.T.; Horváth, I.T. Integration of Homogeneous and Heterogeneous Catalytic Processes for a Multi-step Conversion of Biomass: From Sucrose to Levulinic Acid, γ -Valerolactone, 1,4-Pentanediol, 2-Methyltetrahydrofuran, and Alkanes. *Top. Catal.* **2008**, *48*, 49–54. [[CrossRef](#)]
15. Fernandes, D.R.; Rocha, A.S.; Maia, E.F.; Mota, C.J.A.; da Silva, V.T. Levulinic acid esterification with ethanol to ethyl levulinate production over solid acid catalysts. *Appl. Catal. A Gen.* **2012**, *425*, 199–204. [[CrossRef](#)]

16. Kuwahara, Y.; Kaburagi, W.; Nemoto, K.; Fujitani, T. Esterification of levulinic acid with ethanol over sulfated Si-doped ZrO₂ solid acid catalyst: Study of the structure–activity relationships. *Appl. Catal. A Gen.* **2014**, *476*, 186–196. [[CrossRef](#)]
17. Popova, M.; Shestakova, P.; Lazarova, H.; Dimitrov, M.; Kovacheva, D.; Szegedi, A.; Mali, G.; Dasireddy, V.; Likozar, B.; Wilde, N.; et al. Efficient solid acid catalysts based on sulfated tin oxides for liquid phase esterification of levulinic acid with ethanol. *Appl. Catal. A Gen.* **2018**, *560*, 119–131. [[CrossRef](#)]
18. Huang, Y.B.; Yang, T.; Cai, B.; Chang, X.; Pan, H. Highly efficient metal salt catalyst for the esterification of biomass derived levulinic acid under microwave irradiation. *RSC Adv.* **2016**, *6*, 2106–2111. [[CrossRef](#)]
19. Melero, J.A.; Morales, G.; Iglesias, J.; Paniagua, M.; Hernández, B.; Penedo, S. Efficient conversion of levulinic acid into alkyl levulinates catalyzed by sulfonic mesostructured silicas. *Appl. Catal. A Gen.* **2013**, *466*, 116–122. [[CrossRef](#)]
20. Antunes, M.M.; Lima, S.; Neves, P.; Magalhaes, A.L.; Fazio, E.; Neri, F.; Pereira, M.T.; Silva, A.F.; Silva, C.M.; Rocha, S.M.; et al. Integrated reduction and acid-catalysed conversion of furfural in alcohol medium using Zr,Al-containing ordered micro/mesoporous silicates. *Appl. Catal. B* **2016**, *182*, 485–503. [[CrossRef](#)]
21. Pachamuthu, M.P.; Srinivasan, V.V.; Karvembu, R.; Luque, R. Preparation of mesoporous stannosilicates SnTUD-1 and catalytic activity in levulinic acid esterification. *Microporous Mesoporous Mat.* **2019**, *287*, 159–166. [[CrossRef](#)]
22. Enumula, S.S.; Chada, V.R.B.G.R.R.; Burri, D.R.; Kamaraju, S.R.R. Clean synthesis of alkyl levulinates from levulinic acid over one pot synthesized WO₃-SBA-16 catalyst. *J. Mol. Catal. A Chem.* **2017**, *426*, 30–38. [[CrossRef](#)]
23. Chermahini, A.N.; Nazeri, M. Esterification of the levulinic acid with n-butyl and isobutyl alcohols over aluminum-containing MCM-41. *Fuel Process. Technol.* **2017**, *167*, 442–450. [[CrossRef](#)]
24. Song, D.; An, S.; Sun, Y.; Guo, Y. Efficient conversion of levulinic acid or furfuryl alcohol into alkyl levulinates catalyzed by heteropoly acid and ZrO₂ bifunctionalized organosilica nanotubes. *J. Catal.* **2016**, *333*, 184–199. [[CrossRef](#)]
25. Pileidis, F.D.; Tabassum, M.; Coutts, S.; Ttitirici, M.M. Esterification of levulinic acid into ethyl levulinate catalysed by sulfonated hydrothermal carbons. *Chin. J. Catal.* **2014**, *35*, 929–936. [[CrossRef](#)]
26. Tejero, M.A.; Ramírez, E.; Fité, C.; Tejero, J.; Cunill, F. Esterification of levulinic acid with butanol over ion exchange resins. *Appl. Catal. A Gen.* **2016**, *517*, 56–66. [[CrossRef](#)]
27. Guo, T.; Qiu, M.; Qi, X. Selective conversion of biomass-derived levulinic acid to ethyl levulinate catalyzed by metal organic framework (MOF)-supported polyoxometalates. *Appl. Catal. A Gen.* **2019**, *572*, 168–175. [[CrossRef](#)]
28. Llorente, P.L. Síntesis y Aplicación Catalítica de Materiales MOF en Reacciones de Química Fina. Ph.D. Thesis, Universidad Rey Juan Carlos, Móstoles, Spain, 2017.
29. Stock, N.; Biswas, S. Synthesis of Metal-Organic Frameworks (MOFs): Routes to Various MOF Topologies, Morphologies, and Composites. *J. Am. Chem. Soc.* **2012**, *112*, 933–969.
30. Rowsell, J.L.C.; Yaghi, O.M. Metal–organic frameworks: A new class of porous materials: A Review. *J. Am. Chem. Soc.* **2004**, *73*, 3–14. [[CrossRef](#)]
31. Yujia, S.J.; Hong-Cai, Z. Recent progress in the synthesis of metal–organic frameworks. *Sci. Technol. Adv. Mater.* **2015**, *16*, 54202.
32. Kandiah, M.; Nilsen, M.H.; Usseglio, S.; Jakobsen, S.; Olsbye, U.; Tilsted, M.; Larabi, C.; Quadrelli, E.A.; Bonino, F.; Lillerud, K.P. Synthesis and Stability of Tagged UiO-66 Zr-MOFs. *Chem. Mat.* **2010**, *22*, 6632–6640. [[CrossRef](#)]
33. Abid, H.R.; Shang, J.; Ang, H.M.J.; Wang, S. Amino-functionalized Zr-MOF nanoparticles for adsorption of CO₂ and CH₄. *Int. J. Smart Nano Mater.* **2013**, *4*, 72–82. [[CrossRef](#)]
34. Cao, Y.; Zhang, H.; Song, F.; Huang, T.; Ji, J.; Zhong, Q.; Chu, W.; Xu, Q. UiO-66-NH₂/GO Composite: Synthesis, Characterization and CO₂ Adsorption Performance. *Materials* **2018**, *11*, 589. [[CrossRef](#)]
35. Katz, M.J.; Brown, Z.J.; Colón, Y.J.; Siu, P.W.; Scheidt, K.A.; Snurr, R.Q.; Hupp, J.T.; Farha, O.K. A facile synthesis of UiO-66, UiO-67 and their derivatives. *Chem. Commun.* **2013**, *49*, 9449–9451. [[CrossRef](#)]
36. Cirujano, F.G.; Corma, A.; Xamena, F.X.L.i. Conversion of levulinic acid into chemicals: Synthesis of biomass derived levulinate esters over Zr-containing MOFs. *Chem. Eng. Sci.* **2015**, *124*, 52–60. [[CrossRef](#)]
37. Negus, M.P.; Mansfield, A.C.; Leadbeater, N.E. The preparation of ethyl levulinate facilitated by flow processing: The catalyzed and uncatalyzed esterification of levulinic acid. *J. Flow Chem.* **2015**, *5*, 148–150. [[CrossRef](#)]
38. Peixoto, A.F.; Ramos, R.; Moreira, M.M.; Soares, O.S.G.P.; Ribeiro, L.S.; Pereira, M.F.R.; Delerue-Matos, C.; Freire, C. Production of ethyl levulinate fuel bioadditive from 5-hydroxymethylfurfural over sulfonic acid functionalized biochar catalysts. *Fuel* **2021**, *303*, 121227. [[CrossRef](#)]
39. Tukacs, J.M.; Sylvester, Á.; Kmezc, I.; Jones, R.V.; Óvári, M.; Mika, L.T. Continuous flow hydrogenation of methyl and ethyl levulinate: An alternative route to g-valerolactone production. *R. Soc. Open Sci.* **2019**, *6*, 182233. [[CrossRef](#)] [[PubMed](#)]
40. Lozano, L.; Iglesias, C.; Faroldi, B.; Zamaro, M.U.y.J. Efficient solvothermal synthesis of highly porous UiO-66 nanocrystals in dimethylformamide-free media. *J. Mater. Sci.* **2018**, *53*, 1862–1873. [[CrossRef](#)]
41. Caratelli, C.; Hajek, J.; Cirujano, F.G.; Waroquier, M.; Xamenab, F.X.L.i.; van Speybroeck, V. Nature of active sites on UiO-66 and beneficial influence of water in the catalysis of Fischer esterification. *J. Catal.* **2017**, *352*, 401–414. [[CrossRef](#)]
42. Cirujano, F.G.; Corma, A.; Xamena, F.X.L.i. Zirconium-containing metal organic frameworks as solid acid catalysts for the esterification of free fatty acids: Synthesis of biodiesel and other compounds of interest. *Catal. Today* **2014**, *274*, 213–220. [[CrossRef](#)]
43. Ramli, N.A.S.; Zaharudin, N.H.; Amin, N.A.S. Esterification of renewable levulinic acid to levulinate esters using amberlyst-15 as a solid acid catalyst. *J. Teknol.* **2017**, *79*, 137–142. [[CrossRef](#)]

44. Desidery, L.; Yusubov, M.S.; Zhuiykov, S.; Verpoort, F. Fully-sulfonated hydrated UiO66 as efficient catalyst for ethyl levulinate production by esterification. *Catal. Commun.* **2018**, *117*, 33–37. [[CrossRef](#)]
45. Lin, K.Y.A.; Liu, Y.T.J.; Chen, S.Y. Adsorption of fluoride to UiO-66-NH₂ in water: Stability, kinetic, isotherm and thermodynamic studies. *J. Colloid Interface Sci.* **2016**, *461*, 79–87. [[CrossRef](#)] [[PubMed](#)]
46. Huang, A.; Wan, L.; Caro, J. Microwave-assisted synthesis of well-shaped UiO-66-NH₂ with high CO₂ adsorption capacity. *Mater. Res. Bull.* **2018**, *98*, 308–313. [[CrossRef](#)]
47. Rubio-Martinez, M.; Batten, M.P.; Polyzos, A.; Carey, K.C.; Mardel, J.I.; Lim, K.S.; Hill, M.R. Versatile, High Quality and Scalable Continuous Flow Production of Metal-Organic Frameworks. *Sci. Rep.* **2014**, *4*, 5443. [[CrossRef](#)]
48. Wang, J.; Xia, T.; Zhang, X.; Zhang, Q.; Cui, Y.; Yang, Y.; Qian, G. A turn-on fluorescent probe for Cd²⁺ detection in aqueous environments based on an imine functionalized nanoscale metal-organic framework. *RSC Adv.* **2017**, *7*, 54892–54897. [[CrossRef](#)]
49. Arrozi, U.S.F.; Wijaya, H.W.; Patah, A.; Permana, Y. Efficient acetalization of benzaldehydes using UiO-66 and UiO-67: Substrates accessibility or Lewis acidity of zirconium. *Appl. Catal. A Gen.* **2015**, *506*, 77–84. [[CrossRef](#)]
50. Lu, A.X.; McEntee, M.; Browe, M.A.; Hall, M.G.; DeCoste, J.B.; Peterson, G.W. MOFabric: Electrospun Nanofiber Mats from PVDF/UiO-66-NH₂ for Chemical Protection and Decontamination. *Appl. Mater. Interfaces* **2017**, *9*, 13632–13636. [[CrossRef](#)]
51. Luu, C.L.; van Nguyen, T.T.; Nguyen, T.; Hoang, T.C. Synthesis, characterization and adsorption ability of UiO-66-NH₂. *Adv. Nat. Sci.-Nanosci.* **2015**, *6*, 25004. [[CrossRef](#)]
52. Han, Y.; Liu, M.; Li, K.; Guo, X. Facile synthesis of morphology and size-controlled zirconium metal-organic framework UiO-66: The role of hydrofluoric acid in crystallization. *CrystEngComm* **2015**, *17*, 6434–6440. [[CrossRef](#)]
53. Hou, J.; Luan, Y.; Tang, J.; Wensley, A.M.; Yanga, M.; Lu, Y. Synthesis of UiO-66-NH₂ derived heterogeneous copper (II) catalyst and study of its application in the selective aerobic oxidation of alcohols. *J. Mol. Catal. A Chem.* **2015**, *407*, 53–59. [[CrossRef](#)]
54. Wang, N.; Zhang, G.; Wang, L.; Li, J.; An, Q.; Ji, S. Pervaporation dehydration of acetic acid using NH₂-UiO-66/PEI mixed matrix membranes. *Sep. Purif. Technol.* **2017**, *186*, 20–27. [[CrossRef](#)]
55. Tang, J.; Dong, W.; Wang, G.; Yao, Y.; Cai, L.; Liu, Y.; Tan, L. Efficient molybdenum (vi) modified Zr-MOF catalysts for epoxidation of olefins. *RSC Adv.* **2014**, *4*, 42977–42982. [[CrossRef](#)]
56. Venturi, D.M.; Campana, F.; Marmottini, F.; Costantino, F.; Vaccaro, L. Extensive Screening of Green Solvents for Safe and Sustainable UiO-66 Synthesis. *ACS Sustain. Chem. Eng.* **2020**, *8*, 17154–17164. [[CrossRef](#)]
57. Ploskonka, A.M.; Marzen, S.E.; DeCoste, J.B. Facile Synthesis and Direct Activation of Zirconium Based Metal-Organic Frameworks from Acetone. *Ind. Eng. Chem. Res.* **2017**, *56*, 1478–1484. [[CrossRef](#)]
58. Thommes, M.; Kaneko, K.; Neimark, A.; Olivier, J.; Reinoso, F.R.; Rouquerol, J.; Sing, K. Physisorption of gases, with special reference to the evaluation of surface area and pore size distribution (IUPAC Technical Report). *Pure Appl. Chem.* **2015**, *87*, 1051–1069. [[CrossRef](#)]
59. Groen, J.C.; Peffer, L.A.; Pérez-Ramírez, J. Pore size determination in modified micro- and mesoporous materials. Pitfalls and limitations in gas adsorption data analysis. Review. *Microporous Mesoporous Mat.* **2003**, *60*, 1–17. [[CrossRef](#)]
60. Gomes, I.S.; de Carvalho, D.C.; Oliveira, A.C.; Rodríguez-Castellón, E.; Lang, R. On the reasons for deactivation of titanate nanotubes with metals catalysts in the acetalization of glycerol with acetone. *Chem. Eng.* **2018**, *334*, 1927–1942. [[CrossRef](#)]
61. Travlou, N.A.; Ginnakoudakis, D.A.; Algarra, M.; Labella, A.M.; Rodríguez-Castellón, E.; Badosz, T.J. S- and N-doped carbon quantum dots: Surface chemistry dependent antibacterial activity. *Carbon* **2018**, *135*, 04–111. [[CrossRef](#)]
62. Wang, Y.; Li, L.; Dai, P.; Yan, L.; Cao, L.; Gu, X.; Zhao, X. Missing-node directed synthesis of hierarchical pores on a zirconium metal-organic framework with tunable porosity and enhanced surface acidity via a microdroplet flow reaction. *J. Mater. Chem. A* **2017**, *5*, 22372–22379. [[CrossRef](#)]
63. Moulder, J.F.; Stickle, W.F.; Sobol, P.E.; Bomben, K.D. *Handbook of X-ray Photoelectron Spectroscopy*; Perkin-Elmer Corp: Eden Prairie, MN, USA, 1992.
64. Chakarova, K.; Strauss, I.; Mihaylov, M.; Drenchev, N.; Hadjiivanov, K. Evolution of acid and basic sites in UiO-66 and UiO-66-NH₂ metal-organic frameworks: FTIR study by probe molecules. *Microporous Mesoporous Mat.* **2019**, *281*, 110–122. [[CrossRef](#)]
65. DeStefano, M.R.; Islamoglu, T.; Garibay, S.J.; Hupp, J.T.; Farha, O.K. Room temperature synthesis of uiO-66 and the thermal modulation of densities of defect sites. *Chem. Mat.* **2017**, *29*, 1357–1361. [[CrossRef](#)]
66. Nandiwale, K.Y.; Sonar, S.K.; Niphadkar, P.S.; Joshi, P.N.; Deshpande, S.S.; Patil, V.S.; Bokade, V.V. Catalytic upgrading of renewable levulinic acid to ethyl levulinate biodiesel using dodecatungstophosphoric acid supported on desilicated H-ZSM-5 as catalyst. *Appl. Catal. A Gen.* **2013**, *460*, 90–98. [[CrossRef](#)]
67. Zubir, M.I.; Chin, S.Y. Kinetics of Modified Zirconia-catalyzed Heterogeneous Esterification Reaction for Biodiesel Production. *Appl. Sci.* **2010**, *10*, 2584–2589. [[CrossRef](#)]
68. Jrad, A.; Tarboush, B.J.A.; Hmadeh, M.; Ahmad, M. Tuning acidity in zirconium-based metal organic frameworks catalysts for enhanced production of butyl butyrate. *Appl. Catal. A Gen.* **2019**, *570*, 31–41. [[CrossRef](#)]